MID-INFRARED DUAL-BAND ABSORBER BASED ON NESTED METAMATERIAL STRUCTURE**

Z. Li, J. Li*, Y. Zhang, Y. Zhai, X. Chu, Y. Zhang

International Joint Research Center for Nanophotonics and Biophotonics, Nanophotonics and Biophotonics Key Laboratory of Jilin Province, School of Science at Changchun University of Science and Technology, Changchun, 130022, China; e-mail: lijh@cust.edu.cn

A dual-band metamaterial absorber based on nested nanostructures is proposed. Finite-difference time-domain simulations revealed two resonance absorption peaks with narrow half-widths in the mid-infrared, with center wavelengths at 3.87 and 4.57 μm. The structure exhibited extremely high sensitivity with no polarization sensitivity. Triple-band absorption was observed by controlling the thickness of the top pattern layer. The effects of various metallic materials and geometric structures on the absorption are discussed. The nested infrared-absorbing structure has potential applications in sensors and detectors. Furthermore, multiple absorption peaks via thickness changes provide a theoretical basis for future research on multi-band absorption.

Keywords: *dual-band, metamaterials, mid-infrared, Fabry–Perot resonator.*

ДВУХПОЛОСНЫЙ ПОГЛОТИТЕЛЬ СРЕДНЕГО ИНФРАКРАСНОГО ДИАПАЗОНА НА ОСНОВЕ ВЛОЖЕННОЙ СТРУКТУРЫ ИЗ МЕТАМАТЕРИАЛА

Z. Li, J. Li*, Y. Zhang, Y. Zhai, X. Chu, Y. Zhang

УДК 535.34;620.3

Международный исследовательский центр нанофотоники и биофотоники провинции Цзилинь, Научная школа Чанчуньского университета науки и техники, Чанчунь, 130022, Китай; e-mail: lijh@cust.edu.cn

(Поступила 5 февраля 2021)

Предложен двухзонный поглотитель из метаматериала на основе вложенных наноструктур. Моделирование с использованием метода конечных разностей во временной области выявило два пика резонансного поглощения с узкой полушириной в средней ИК-области с центральными длинами волн 3.87 и 4.57 мкм. Структура показала чрезвычайно высокую чувствительность в отсутствие поляризационной чувствительности. Трехполосное поглощение наблюдали, контролируя толщину верхнего слоя рисунка. Обсуждается влияние различных металлических материалов и геометрических структур на поглощение. Вложенная структура, поглощающая ИК-излучение, может найти применение в датчиках и детекторах. Множественные пики поглощения при изменении толщины обеспечивают теоретическую основу для исследований многополосного поглощения.

Ключевые слова: *двухдиапазонный метаматериал, средний ИК-диапазон, резонатор Фабри–Перо.*

Introduction. Artificial metamaterials (MMs) have been receiving considerable attention because of negative refractive indices [1], perfect light absorption [2], and extraordinary optical transmission [3]. In particular, a MM perfect absorber (MMPA), which was first demonstrated by Landy et al. [4], exhibits high absorption characteristics, tunable resonant frequencies, and high Q-factors. Normal absorption is based on material characteristics, while a MM structure is a sub-wavelength specific resonator [5]. High absorption has been demonstrated for radio waves [6], microwaves [7], millimeter-waves [8], terahertz frequencies [9], and

**Full text is published in JAS V. 88, No. 6 (http://springer.com/journal/10812) and in electronic version of ZhPS V. 88, No. 6 (http://www.elibrary.ru/title_about.asp?id=7318; sales@elibrary.ru).

various infrared bands [10–12]. Because of their approximately unity absorbance, MMPAs have become attractive for optoelectronic applications, such as detectors [13], emitters [14], imaging equipment [15], and solar cells [16]. Infrared detectors based on MMs have exhibited ultra-fast responsivities and significantly high signal-to-noise ratios [17]. Due to limiting size effects, normal absorbing structures often have large half-widths, which result in lower sensitivity [18]. The nested structure discussed here can overcome the size effect for narrowband absorption in the mid-infrared region. The peak width derives from dual-band absorption and the sensitivity is extremely high. Thus, it has great application potential in detectors and frequency selectors.

We propose a narrow dual-band, high-quality MMPA with very high selectivity based on a nested double-cross stack. In simulations, we used a single unit cell in the propagation direction to obtain two peaks with average absorptions of up to 99%, with a thickness significantly less than the resonant wavelength. The scalability of the wavelength enables applications such as bolometric pixel elements and thermoelectric detectors. The design is extremely useful for narrow-band-responsive bolometers used as focal-plane-array imaging detectors. The detector can also be used for flammable, toxic, and harmful gases such as CH_4, CO, and C_2H_6 in the mid-infrared region and SO_2F_2 and SF_6 in the far-infrared region [19]. It can also be used in thermal imaging [20], hyperspectral imaging [21], meteorology [22], free-space light [23], communication [24], remote sensing [25], lasers [26], and for identifying biological compounds [27].

Model and method. In the nested MM structure, the top layer is a periodic-array cross structure. The middle layer is a silica dielectric, and the substrate is silicon. There is an additional cross array structure in the middle of the silica dielectric layer that is the same as that in the top layer. A continuous metal film blocks transmission of mid-infrared electromagnetic waves, so that incident waves are completely reflected and not transmitted. This structure is similar to a Fabry-Perot resonator. The resonance absorption peak of the specific structure in the top layer can match the spatial electromagnetic wave perfectly. The silica layer plays a normal selective role. The cross structure in the middle of the dielectric layer can absorb long-wavelength electromagnetic waves. The light source used in the simulations was a plane wave incident in a vertical direction. L = 1 μm and W = 1 μm represent the arm length and width of the cross structure, respectively.

In the numerical simulations, we used finite-difference time-domain (FDTD) methods to solve Maxwell's equations and obtain electric and magnetic field intensities of the surface plasmon resonance of the excitation. The absorption and reflection spectra in the direction perpendicular to an incident electromagnetic wave can be obtained with relation [28–30]:

$$T_\lambda = \int S(x, y)dxdy/Q_{\lambda,i}, \tag{1}$$

where Q is the incident electromagnetic field power per unit area, $S(x,y) = \int_0^T |\mathbf{E} \times \mathbf{H}| dt / T$ is the Poynting vector, and T is the surface plasmon resonance period. Absorption and transmission peaks can be modeled with Eq. (1). Definition A represents the absorbance, where the surface plasmon resonance absorption loss of the incident electromagnetic wave can be defined as:

$$A = 1 - T - R. \tag{2}$$

Numerical analysis and discussion. The geometry of the optimized structure in Fig. 1a was controlled by adjusting the eight variables in Fig. 1b. By changing t_1, t_2, t_3, t_4, and t_5, the thicknesses of the dielectric layer and the metal cross structure layer were changed; T represents the period of the nested structure, and, as noted above, L and W control the cross structures arm length and arm width, respectively.

Perfect absorber nested structure. The unit cell of the nested structure is shown in Fig 1. The geometric size of the structure was $L = W$ = 1 μm, t_1 = 0.15 μm, t_2 = 0.65 μm, t_3 = 0.6 μm, t_4 = 0.25 μm, t_5 = 0.2 μm, and T = 3 μm. FDTD simulation optimization resulted in two mid-infrared resonance absorption peaks with narrow half-widths, as shown in Fig 2. The center wavelengths were at 3.87 and 4.57 μm, respectively. In the simulations, the light source was a plane wave, and the dispersion parameters of the various materials are all from Palik experimental data in the mid-infrared, and the spatial background index of the structure was set to 1.

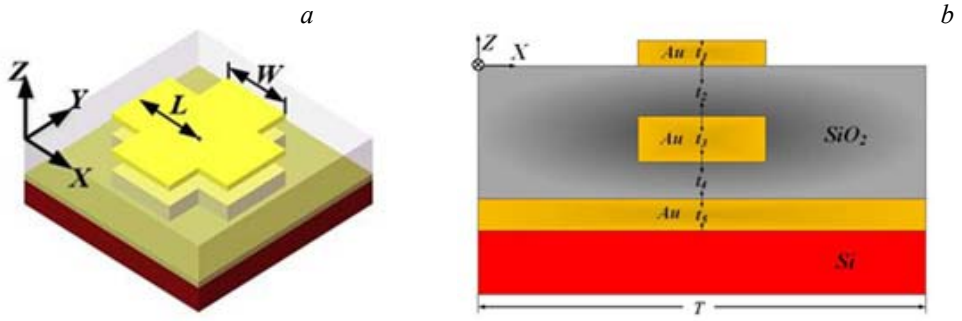

Fig. 1. Unit cell of the proposed nested structure (a) perspective view (b) bottom view; $t_1 = 0.15$ μm, $t_2 = 0.65$ μm, $t_3 = 0.6$ μm, $t_4 = 0.25$ μm, $T = 3.0$ μm in the picture (b).

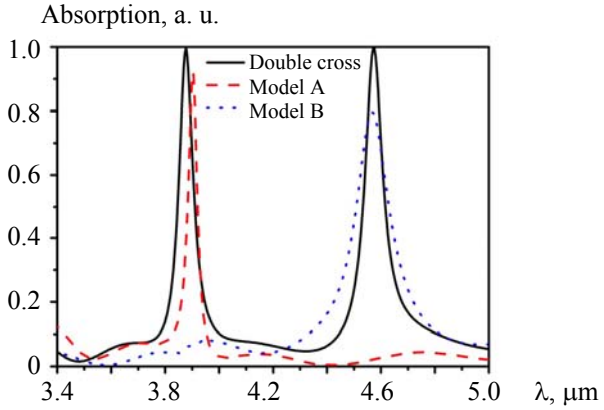

Fig. 2. Simulated absorption peaks of the nested structure; $t_1 = 0.15$ μm, $t_2 = 0.65$ μm, $t_3 = 0.6$ μm, $t_4 = 0.25$ μm, $T = 3.0$ μm.

To analyze the absorption mechanism, the FDTD software was used to simulate the electric-field and Poynting vector distributions, as shown in Figs. 3 and 4, respectively. From these distributions, a conclusion could be made that the 3.87-μm resonance absorption peak was attributed to the double-layer cross structure. It equivalently formed an electric-dipole pair from the incident electromagnetic wave electric vector on the top metal cross. The electromagnetic wave energy was completely converted into an ohmic loss of the overall electronic oscillation. At 4.57 μm, via the energy propagation direction shown in Fig 4, the electromagnetic wave directly penetrated the dielectric layer and impedance-matched the internal metal cross. It thereby introduced the spatial electromagnetic wave into the dielectric layer between the nested cross and the bottom metallic layer. This part of the energy loss was absorbed by the dielectric.

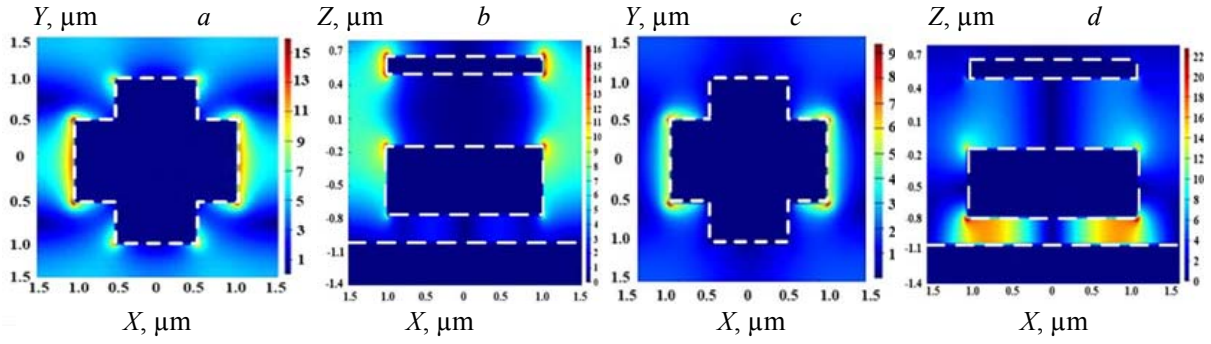

Fig. 3. Top views of the calculated electromagnetic field distributions for the (a,b) 3.87 and (c,d) 4.57 μm peak.

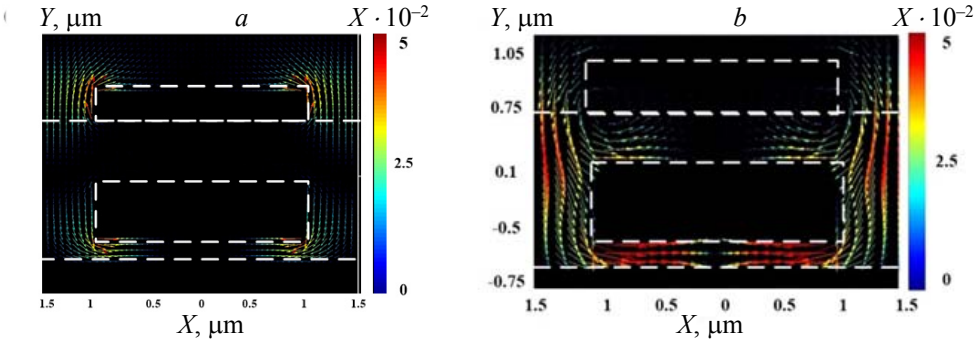

Fig. 4. Calculated Poynting vector distributions at (a) 3.87 and (b) 4.57 μm.

Effect of the cross scale in the top nested structure on the absorptive properties. From the absorption analysis, it was concluded that energy loss was concentrated at the two ends of the metal cross structure and the inside of the dielectric layer between the nested cross structure and the bottom metal barrier layer. Therefore, change the size of the metal cross structure and the thickness of the bottom dielectric layer (L and t_4) had a significant impact on the absorption effect. Because the top cross and the nested cross form an equivalent electric-dipole pair, the wavelength of the resonance absorption peak was affected by the oscillation frequency of the dipole pair. Therefore, when the arm length and width of the cross structure were reduced, the electric-dipole moment was reduced, the oscillation frequency was increased, and the resonance absorption peak was blue-shifted. When the arm length and width were increased, the electric-dipole moment increased, and the resonance absorption peak red-shifted.

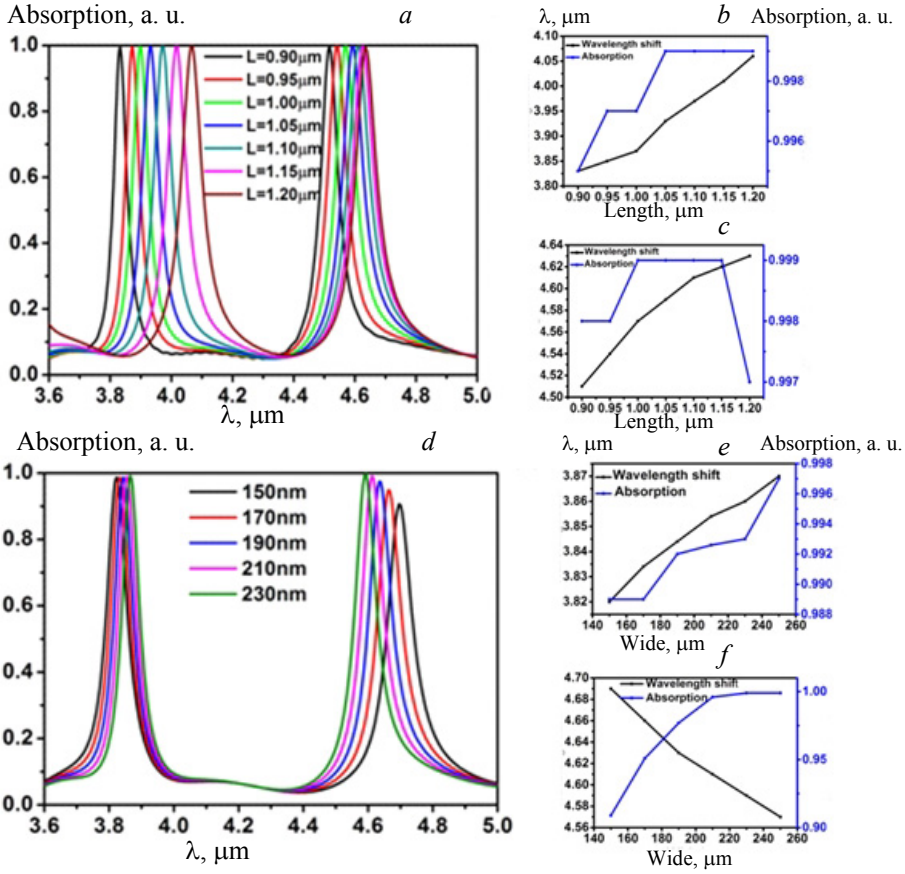

Fig. 5. For fixed $t_1 = 0.15$ μm, $t_2 = 0.65$ μm, $t_3 = 0.6$ μm, $t_4 = 0.25$ μm, $T = 3.0$ μm; (a) absorption spectra with changing arm length and width; (b,c) absorption intensity and absorption peak frequency shift, respectively; (d) absorption spectra with changing thicknesses of the dielectric layer; (e,f) absorption intensity and absorption peak frequency shift, respectively.

It can be concluded from the energy distribution of the field that the resonance absorption peak at 4.57 μm was caused by loss of the dielectric layer between the bottom metallic layer and the bottom of the nested cross structure, as shown in Fig. 5. When the thickness of the middle dielectric layer decreased, the 3.87-μm resonance absorption peak did not change significantly, while the 4.57 peak had a significant red-shift, and the absorption intensity decreased significantly. The absorption intensity was reduced because of the thinned dielectric layer. The red-shift of the absorption peak was attributed to the fact that long-wavelength electromagnetic waves were more likely to be diffracted and introduced into the dielectric layer.

Effect of the adjacent nested-structure period on mid-infrared absorption. Changing the periodicity of the adjacent nested structures affected the absorptive properties. First, the structural parameters were fixed at t_1 = 0.15 μm, t_2 = 0.65 μm, t_3 = 0.6 μm, t_4 = 0.25 μm, and T = 3.0 μm, in addition to the structural periodic parameters. The simulated absorption properties demonstrated that the absorption intensity changed significantly when the periodic structure parameter was changed. When the periodic structure parameter was 3.0 μm, the absorption was close to 100%. When the parameter was less than 3.0 μm, the absorption decreased (Fig. 6). The unit period variable was 100 nm. When the period decreased, the duty ratio increased, and the resonant absorption peak had a significant blue-shift, indicating that the interaction between the adjacent electromagnetic fields increased and the resonance frequency increased. The reason for the decreased intensity was because of the changed periodicity of the structure. The balance of impedance matching was then disrupted, resulting in a decreased absorption intensity.

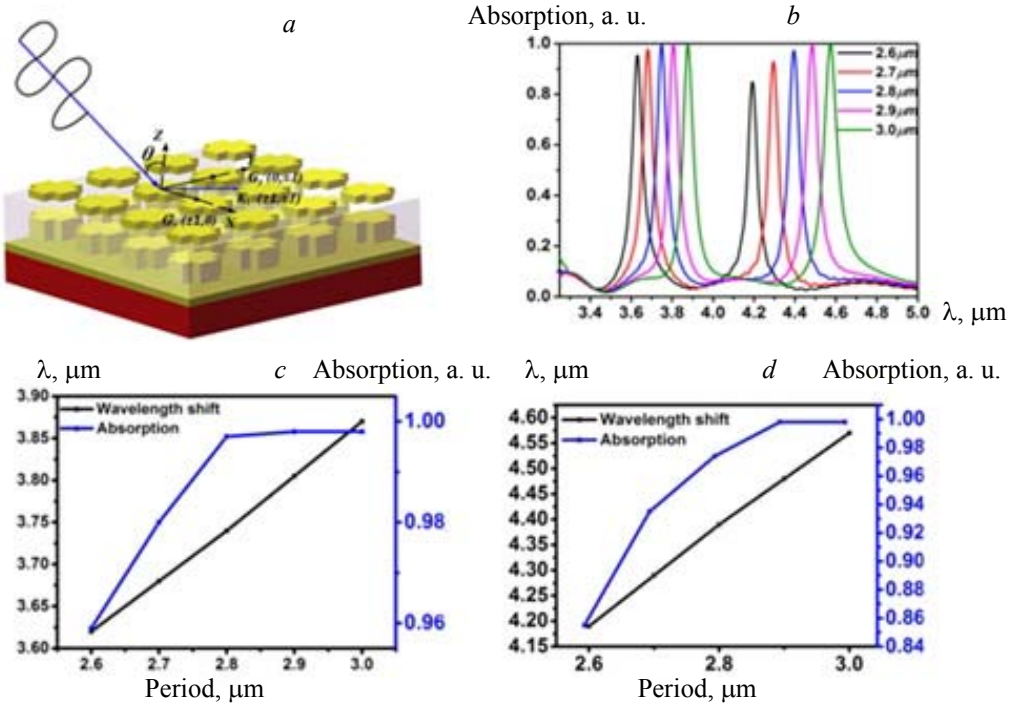

Fig. 6. For fixed t_1 = 0.15 μm, t_2 = 0.65 μm, t_3 = 0.6 μm, t_4 = 0.25 μm, T = 3.0 μm, and a changing period from 2.6 to 3.0 μm; (a) schematic of the structure; (b) spectra produced by periodic changes; (c) and (d) are plots of the peaks at 3.87 and 4.57 μm, respectively.

Effect of nested-structure polarization on mid-infrared absorption. Additional simulations investigated the angle-dependence of the dual-band plasmonic absorber. Because there was a phase shift in the incident electromagnetic field between each period, we used Bloch boundary conditions for oblique polarizations in the x-direction (propagation direction) for both transverse electric and magnetic polarizations, while maintaining all the other parameters. Figure 7 displays the absorptivity as a function of both wavelength and the polarization angle. The two red regions indicated two sharp angle-independent absorption bands. Under both transverse electric and magnetic polarizations, more than 95% absorption was observed for both resonance peaks, while maintaining the center frequencies to reveal the decreased absorption peak values between normal incidences.

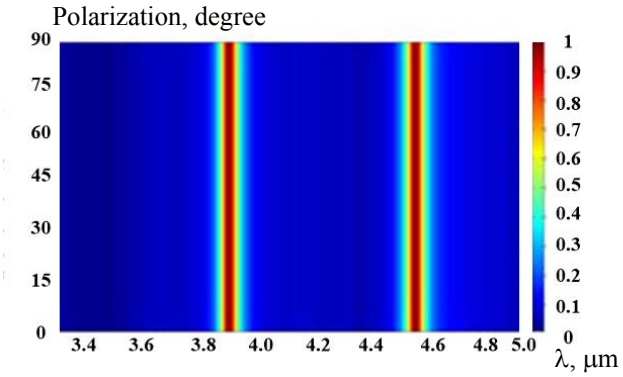

Fig. 7. Simulated absorption efficiencies as a function of wavelength and polarization angle; 3.5 simulation of the nested structure sensitivity.

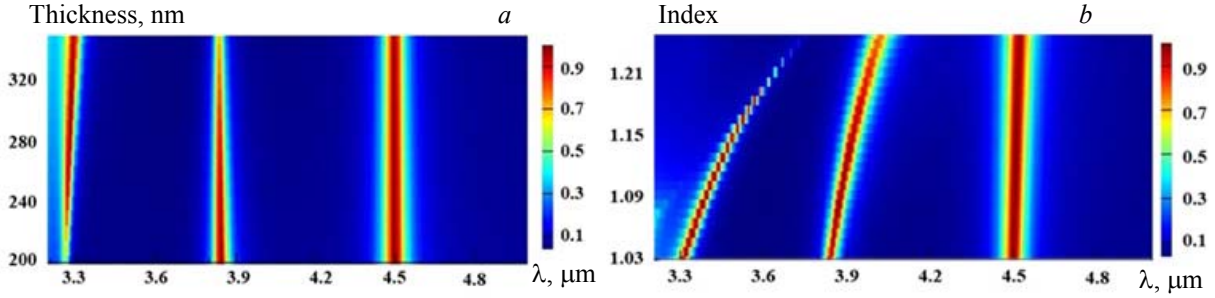

Fig 8. (a) Absorption spectra with the variable thickness of the top cross-pattern layer; (b) absorption spectra with the variable background refractive index, for a 250-nm-thick top cross.

By changing the thickness of the top-layer cross, the simulations produced a new absorption peak at 3.26 μm, as shown in Fig. 8a. To find the most suitable cross thickness over the range 200–320 nm, the results were fitted. In Fig. 8a, the 3.26 μm peak appeared when the cross thickness was increased. When it was greater than 300 nm, the absorption efficiency at 3.87 μm was reduced. When it was less than 250 nm, the 3.26-μm absorption disappeared. In Fig. 8b, for a fixed the top layer cross thickness of 250 nm, the results are shown when the background index was changed. This affected the top cross because it was in the external medium, while the intermediate-layer cross was always embedded in silica. The background refractive index changes did not generate a resonance absorption in the intermediate-layer cross. Therefore, the peaks at 3.87 and 3.26 μm were significantly red-shifted when the index ranged over 1.025–1.25. The peak at 4.57 μm was hardly affected by altering the index. Continuous tunability of the short-wavelength resonance absorption peaks was thus possible.

Conclusions. FDTD optimization of a proposed MMPA nested structure produced two mid-infrared resonance absorption peaks at 3.87 and 4.57 μm, with narrow half-widths. The absorption mechanism was simulated, also using FDTD. Three-band absorption was observed for the nested structure by changing the thickness of the top pattern layer. This verified that the device was extremely sensitive with respect to absorption, but it had no polarization sensitivity. Overall, the structure provides a theoretical basis for the perfect absorption of narrow multiple bands in the mid-infrared, with very promising potential applications in detectors and sensors.

Acknowledgements. This work is supported by the Project of China (D17017), the National Natural Science Foundation of China (21703017), the Developing Project of Science and Technology of Jilin Province (202002040JC, 20200201266JC, 20200201271JC, 20200201060JC, 20200201255JC, 20190201181JC), the International Science and Technology Cooperation Project of Jilin Province (20190701029GH), and the Project of Education Department of Jilin Province (JJKH20190551KJ, JJKH20200730KJ), the China Postdoctoral Science Foundation (2019M651181), and the Youth Fund and Technology Innovation Fund of Changchun University of Science and Technology (XQNJJ-2018-03, XJJLG-2018-01).

We thank Alan Burns, PhD, from Liwen Bianji (Edanz) (www.liwenbianji.cn/) for editing the English text of a draft of this manuscript.

REFERENCES

1. J. B. Pendry, *Phys Rev Lett*., **85**, No. 18, 3966–3969 (2000).
2. N. Liu, M. Mesch, T. Weiss, et al., *Nano Lett*., **10**, No. 7, 2342–2348 (2010).
3. W. Chen, N. I. Landy, K. Kempa, W. J. Padilla, *Adv. Opt. Mater*., **1**, No. 3, 195 (2013).
4. N. I. Landy, S. Sajuyigbe, J. J. Mock, et al., *Phys Rev Lett*., **100**, No. 20, 207402 (2008).
5. D. Benedikovic, M. Berciano, Alonso-Ramos, et al., *Opt. Express*, **25**, No. 16, 19468–19478 (2017).
6. N. P. Johnson, A. Z. Khokhar, H. M. Chong, *Opto-Electron. Rev*., **14**, No. 3, 187–191 (2006).
7. Kim Taehwan, Bae Ji-Yeul, Lee Namkyu, et al., *Adv. Funct. Mater*., **73**, No. 19, 1–8 (2018).
8. Xun jun He, Liang Qiu, Yue Wang, et al., *J. Infrared Milli Terahz Waves*, **32**, No. 7, 902–913 (2011).
9. G. Duan, J. Schalch, X. Zhao, J. Zhang, et al., *Opt. Express*, **26**, No. 3, 2242–2251 (2018).
10. L. Zhigang, S. Liliana, D. A. Czaplewski, et al., *Opt. Express*, **26**, No. 5, 5616–5631 (2018).
11. J. Yang, C. Xu, S. Qu, et al., *J. Adv. Dielectrics*, **8**, No. 1, 1850007(1–8) (2018).
12. L. Zhao, H. Liu, Z. He, et al., *Opt. Commun*., **420**, 95–103 (2018).
13. J. Schalch, G. Duan, X. Zhao, X. Zhang, R. D. Averitt, *Appl. Phys. Lett*., **113**, No. 6, 61113 (2018).
14. J. A. Mason, S. Smith, D. Wasserman, et al., *Appl. Phys. Lett*., **98**, No. 24, 241105 (2011).
15. Z. Zhou, T. Zhou, S. Zhang, Z. Shi, Y. Chen, et al., *Adv. Sci.* (Weinh.), **5**, No. 7, 1700982 (2018).
16. L. Lei, L. Shun, H. Haixuan, et al., *Opt. Express*, **26**, No. 5, 5686–5693 (2018).
17. Z. Lei, L. Han, H. Zhihong, et al., *Opt. Express*, **26**, No. 10, 12838–12851 (2018).
18. L. Guo, X. Ma, Y. Zou, et al., *Opt. Laser Technol*., **98**, 247–251 (2018).
19. Rodrigo Sergio G, Martín-Moreno Luis, *Opt. Lett*., **41**, No. 2, 293–296 (2018).
20. Zhao Xiaoguang, Duan Guangwu, Wu Ke, S. W. Anderson, Zhang Xin, *Adv. Mater*., **5**, No. 4, 61–68 (2019).
21. Bhardwaj Amit, Sridurai Vimala, Puthoor Navas Meleth, et al., *Adv. Opt. Mater*., **1**, No. 8, 42–51 (2019).
22. R. Singh, C. Rockstuhl, W. Zhang, *Appl. Phys. Lett*., **97**, No. 24, 241108 (2010).
23. K. Chen, R. Adato, H. Altug. *ACS nano*., **6**, No. 9, 7998–8006 (2012).
24. C. Luo, F. Ling, G. Yao, et al., *Opt. Express*, **24**, No. 2, 1518–1527 (2016).
25. Su Yuanyan, Chen Zhi Ning, *IEEE Transact. Antenn. Propagation*, **1**, 1 (2019).
26. Yang Yu Fan, Hu Han Wen, et al., *Adv. Opt. Mater*., **1**, No. 3, 26–33 (2020).
27. Bai Zhongyang, Liu Yongshan, et al., *ACS Appl. Mater. Interfaces*, **10**, No. 20, 8543 (2020).
28. M. Born, E. Wolf, *Principle of Optics*, Cambridge University (1999).
29. R. C. Rumpf, *Prog. Electromag. Res. B*, **35**, No. 1, 241–261 (2011).
30. L. Li, *J. Opt. Soc. Am. A*, **14**, No. 10, 2758–2767 (1997).